


## Article

# Comprehensive Improvement of Mixed-Flow Pump Impeller Based on Multi-Objective Optimization

Mengcheng Wang , Yanjun Li \*, Jianpin Yuan, Fan Meng, Desmond Appiah and Jiaqi Chen

Research Center of Fluid Machinery Engineering and Technology, Jiangsu University, Zhenjiang 212013, China; jdwmc2018@163.com (M.W.); yh@ujs.edu.cn (J.Y.); mengf2456@126.com (F.M.); bembo88donk@yahoo.com (D.A.); 2111911012@stmail.ujs.edu.cn (J.C.)

\* Correspondence: lyj782900@ujs.edu.cn

Received: 19 June 2020; Accepted: 29 July 2020; Published: 31 July 2020



**Abstract:** The spanwise distribution of impeller exit circulation (SDIEC) has a significant effect on the impeller performance, therefore, there is a need for its consideration in the optimization design of mixed-flow pumps. In this study, a combination optimization system, including a 3D inverse design method (IDM), computational fluid dynamics (CFD), Latin hypercube sampling (LHS) method, response surface model (RSM), and non-dominated sorting genetic algorithm (NSGA-II) was used to improve the performance of the mixed-flow pump after considering the effect of SDIEC on the performance of the impeller. The CFD results confirm the accuracy and credibility of the optimization results because of the good agreement the CFD results established with the experimental measurements. Compared with the original impeller, the pump efficiency of the preferred impeller at  $0.8Q_{des}$ ,  $1.0Q_{des}$ , and  $1.2Q_{des}$  improved by 0.63%, 3.39%, and 3.77% respectively. The low-pressure region on the blade surface reduced by 96.92% while the pump head difference was less than 1.84% at the design point. In addition, a comparison of the flow field of the preferred impeller and the original impeller revealed the effect of SDIEC on mixed-flow pump performance improvement and flow mechanism.

**Keywords:** mixed-flow pump; multi-objective optimization; computational fluid dynamics; 3D inverse design; circulation

## 1. Introduction

The amount of energy consumed by various pumps accounts for more than 12% of the total energy consumption every year. The mixed-flow pumps are increasingly being used in industrial processes and agriculture due to their efficient hydraulic performance. Therefore, it is necessary to provide a reliable and effective optimization design method for further improving the performance of the mixed-flow pump.

The current and commonly used impeller combination optimization system is composed of the following five parts: Impeller geometric parameters, computational fluid dynamics (CFD) analyses, design of experiment (DOE), approximate model and optimization algorithm. The geometric parameters are used to describe the spatial shape of the impeller; CFD is used to calculate the performance of the impeller; DOE is used to create the database samples; the approximate model is used to construct the function relationship between the design variables and optimization objectives, and the optimization algorithm is used to solve the approximate model to obtain an optimal solution set in the entire design space. The effectiveness of this optimization system has been verified in a large number of optimization designs. Suh et al. [1] improved the efficiency and cavitation performance of a mixed-flow pump at the design point by combining the use of the central composite design (CCD), RSM, and sequence quadratic program (SQP) to change the impeller geometric parameters. Kim et al. [2], also solved the

head oversized problem and improved the efficiency of a mixed-flow pump at design point by combined application of CCD and RSM to modify the impeller and diffuser inlet angle. Furthermore, Pei et al. [3] enlarged the high efficiency area of a centrifugal pump by combined using the LHS method, RSM, and NSGA-II to change the meridional shape. The stability, efficiency, and cavitation performance of a centrifugal pump were improved by combined applications of LHS, kriging model, and NSGA-II to modify the meridional shape [4,5]. Miao et al. [6] increased the efficiency and cavitation performance of axial-flow pump by combined usage of Group method of data handling type neural networks and modified PSO to improve the meridional shape. Meng et al. [7] optimized the reversible axial-flow pump by increasing the reverse pump performance with a slight decrease in the forward pump performance by combining LHS, artificial neural network (ANN) and NSGA-II to improve the main geometric parameters of impeller and diffuser.

However, this optimization system is associated with challenges such as, to accurately describe the 3D shape of the impeller, a large number of geometric parameters are required. Moreover, there exists no direct relationship between the geometric parameters and the hydraulic performance of the impeller [8]. Although the sensitivity tests can be used to reduce the number of design parameters, the upper limit of the optimization design drops accordingly. Therefore, a more suitable method of impeller parameterization is needed.

A feasible solution to this problem is to use the IDM to parameterize the impeller [9–11]. The three main design parameters in IDM are the blade loading along the meridional shape at the hub and shroud, the stacking at the trailing edge of the blade, and the circulation along the spanwise at the exit of the impeller. Compared with the traditional parameterization method based on geometry parameters, the IDM has the advantages of fewer design parameters and the design parameters are more closely related to the hydrodynamic performance [12,13]. In addition, the blade angle in IDM is directly computed by the given design parameters, which is quite different from the results obtained by the conformal transformation in the traditional design [14]. The effectiveness of IDM has been widely proven in the optimization design of various turbomachinery. Zhu et al. [15–17] improved the efficiency, cavitation and stability performance of a pump-turbine runner by varying the blade loading and stacking by combined using the LHS, RSM, and NSGA-II. Bonaiuti et al. [18] increased the high efficiency area of a compressor by changing the blade loading, stacking and spanwise circulation by combined using DOE and RSM. Lee et al. [19] improved the efficiency and pressure rise of an axial fan by considering the blade loading, stacking and spanwise circulation by the combined application DOE and RSM.

There is a common point in the previous studies which is, a constant value of circulation from hub to shroud (free vortex) is imposed at impeller exit, and only a few studies used a linear spanwise distribution (forced vortex) at the impeller exit. However, Lang et al. [20] and Chen [21] through the theoretical derivations show that the best spanwise distribution of impeller exit circulation (SDIEC) is a non-linear distribution. Zhang et al. [22,23] proved the correctness of the theoretical derivation through the experimental measurement of a series of high-efficiency pumps. The author's previous work also showed that in the multi-points and multi-objective optimization of mixed-flow pump impeller, there are some better non-linear SDIEC than the linear distribution.

In this study, a widely used mixed-flow pump impeller is comprehensively improved by using the combination optimization system based on IDM after considering the effect of SDIEC on the impeller performance. Firstly, the mixed-flow pump design specifications and the optimization design system are introduced. Secondly, the optimization system was applied to design a series of impeller and a preferred impeller was selected. Finally, the flow field characteristics in the preferred impeller and the original impeller are compared, and the main effect of each parameter to the optimization objective was analyzed.

## 2. Mixed-Flow Pump Model

The mixed-flow pump which is widely used in the South-to-North Water Diversion Project was selected as the original model as shown in Figure 1. The performance of this model has been verified by a large number of experiments. The design specifications of this model are listed in Table 1, and the specific speed  $n_s$  was calculated by:

$$n_s = \frac{3.65NQ^{0.5}}{H^{0.75}} \quad (1)$$

where  $H$  is the head,  $N$  is the rotational speed,  $Q$  is the volume flow rate.

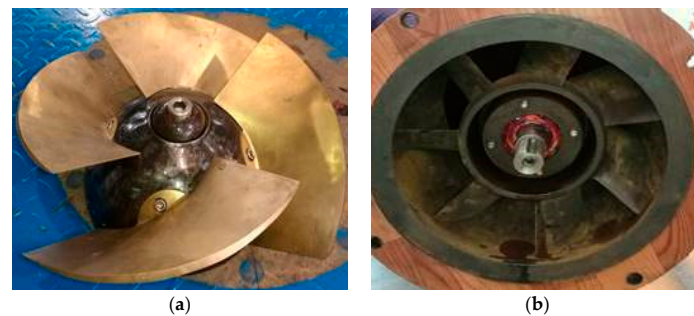


Figure 1. Original model of mixed-flow pump: (a) Impeller; (b) vane diffuser.

Table 1. Design specifications of impeller.

Design Flow Rate (m <sup>3</sup> /s)	0.427	Impeller Blade Number	4
Head on Design Points (m)	12.66	Impeller Diameter (mm)	320
Rotational Speed (r/min)	1450	Specific Speed	511

## 3. Optimization Design System

The combination optimization system was constructed by the CFD analyses, IDM, LHS, RSM, and NSGA-II. The flow chart of this optimization system is shown in Figure 2.

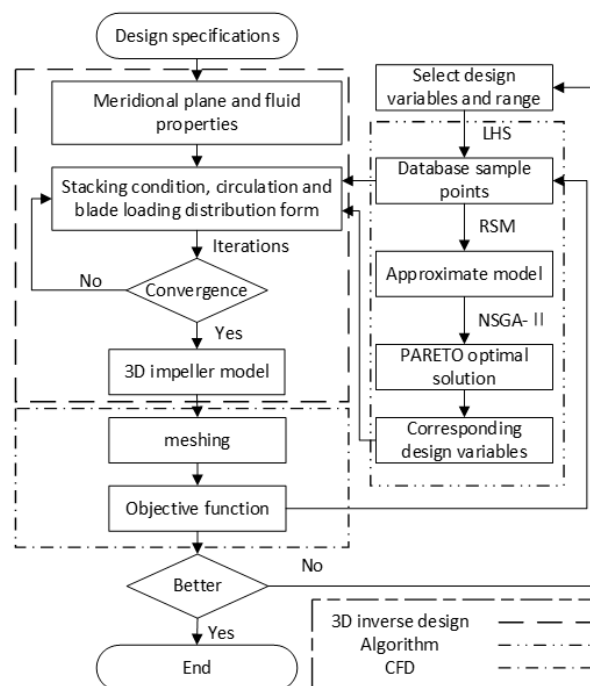


Figure 2. Optimization design system.

### 3.1. CFD Analyses

In this system, CFD analyses were employed to calculate the optimization objectives and validate the results of optimization. Thus, how to ensure the accuracy of CFD analyses become a key point for the optimization process. The widely used commercial software ANSYS (2019 R3, AnShiYaTai, Beijing, China) which is a large-scale general finite element analyses (FEA) software was utilized for performance estimation and inner flow-field analyses.

Structured grids were used in all calculation domains as shown in Figure 3. The structured grids of the impeller and vane diffuser were generated by ANSYS TurboGrid while that of the inlet and outlet pipes were generated by ANSYS ICEM. The pump efficiency and head at design point were selected for the grid independence analysis (See Table 2). Considering the effect of the number of grids on the accuracy of calculation results and the computational resources available, Mesh 3 is adopted for the CFD simulations. Meanwhile, the maximum  $Y^+$  of impeller and diffuser blade surface does not exceed 40 as shown in Figure 3.

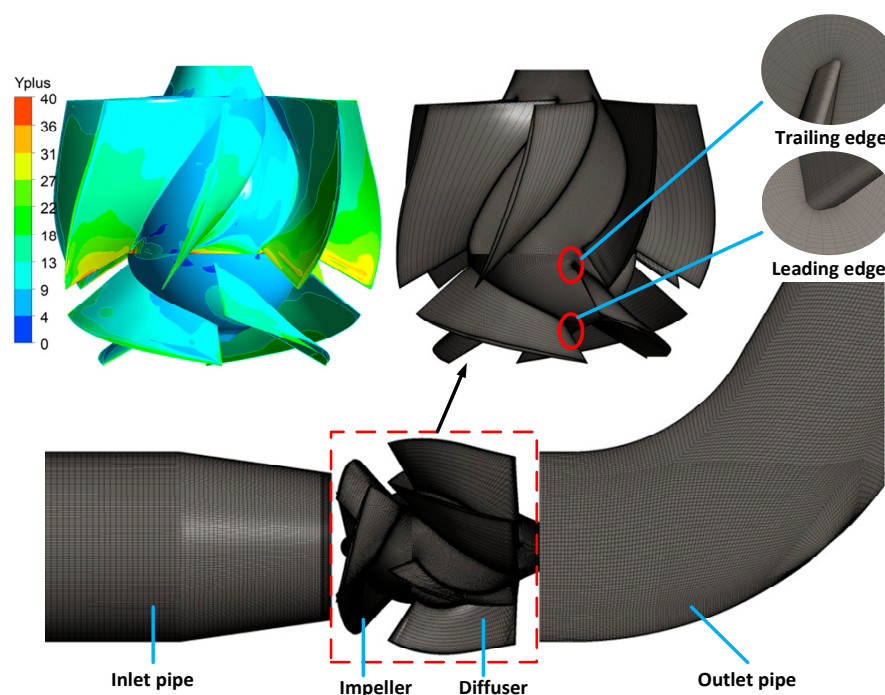


Figure 3. Structured grids of the computational domains.

Table 2. Grid Independence check.

Inflow Pipe ( $\times 10^4$ )	Outflow Pipe ( $\times 10^4$ )	Impeller ( $\times 10^4$ )	Vane Diffuser ( $\times 10^4$ )	Total Mesh ( $\times 10^4$ )	Efficiency (%)	Head (m)
27	49	42	48	166	83.828	12.064
58	67	84	92	301	84.647	12.146
83	95	141	152	471	85.208	12.103
129	142	211	268	750	85.206	12.096

The 3D Reynolds-Averaged Navier–Stokes (RANS) equations and energy equations were used to analyze the incompressible flows in the pump. The governing equations were discretized by the finite volume method. The  $k - \omega$  shear stress transport (SST) model was selected as a closure of the RANS equation since it can accurately predict the flow separation in the pump [24]. The convection–diffusion equation was solved by a high-resolution scheme. “Mass Flow Rate” was set at the inlet boundary while ‘Static Pressure’ was set at outlet boundary. “Frozen rotor” was set at interfaces between the inlet pipe to impeller and impeller to vane diffuser. The no-slip condition was applied to all walls and the Root mean square residual values of mass and all directions of the momentum were set as  $5 \times 10^{-5}$ .

### 3.2. 3D Inverse Design Method

In IDM (Turbodesign 6.4.0, ADT, Shanghai, China, 2020), the inlet flow is considered to be steady, inviscid and uniform, the blades were represented by sheets of vorticity and the vorticity strength was related to the distribution of circumferentially averaged swirl velocity (circulation)  $r\overline{V}_\theta$ :

$$r\overline{V}_\theta = \frac{B}{2\pi} \int_0^{2\pi} rV_\theta d\theta \quad (2)$$

where  $r$  is radius;  $B$  is blade numbers.

Once  $r\overline{V}_\theta$  and other design parameters were known, the blade shape and corresponding flow field can be calculated as shown in Figure 4. The pressure distribution at the blade surface and the blade shape [9] can be calculated by Equations (3) and (4) respectively.

$$\Delta p = p^+ - p^- = \frac{2\pi}{B} \rho W_m \frac{\partial r\overline{V}_\theta}{\partial m} \quad (3)$$

$$(\overline{V}_z + v_{zbl}) \frac{\partial f}{\partial z} + (\overline{V}_r + v_{rbl}) \frac{\partial f}{\partial r} = \frac{r\overline{V}_\theta}{r^2} + \frac{v_{\theta bl}}{r} - \omega \quad (4)$$

where  $p^+$  is the static pressure at the blade work surface;  $p^-$  is the static pressure at the blade suction surface;  $\rho$  is the fluid density;  $W_m$  is the relative velocity on the blade surface;  $m$  represents streamline in the meridional shape and  $m = 0$  means at the blade leading edge,  $m = 1$  means at blade trailing edge.  $\overline{V}_z$  and  $\overline{V}_r$  are the axial and radial components of the circumferential average absolute velocity, respectively;  $v_{zbl}$ ,  $v_{rbl}$ , and  $v_{\theta bl}$  are the axial, radial and circumferential components of periodic velocity, respectively;  $f$  is wrap angle and can be calculated through integration along the streamline, the initial wrap angle  $f^0$  was prescribed by stacking condition which could specify the blade lean at trailing edge as shown in Figure 5.

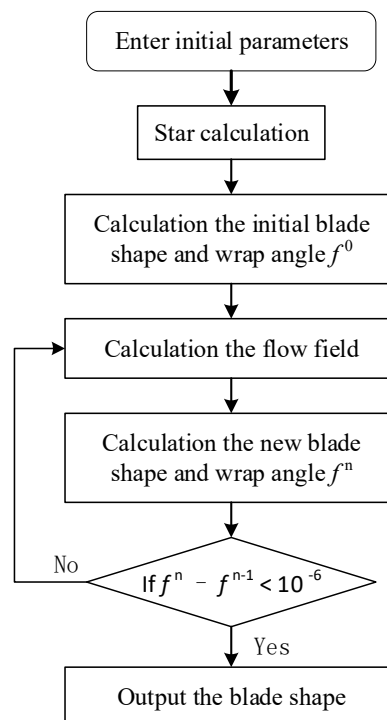
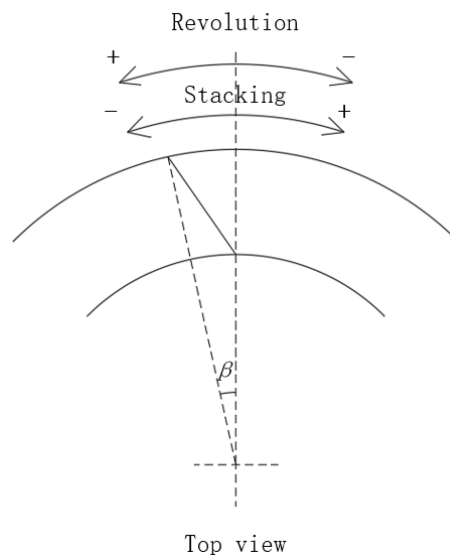


Figure 4. Inverse design method (IDM) calculation flow chart.



**Figure 5.** Stacking condition.

To obtain the impeller model, the following parameters need to be provided.

1. Design specifications and fluid properties.
2. Meridional shape.
3. Spanwise distribution of  $r\overline{V}_\theta$  at the impeller exit.
4. The meridional derivative of the circulation  $\partial(r\overline{V}_\theta)/\partial m$  (blade loading) at the hub and shroud.
5. Stacking condition.

### 3.3. Optimization Process

Construction of the approximate function between the design parameters and optimization objective is important in the optimization process. In this study, the approximate function is established by RSM using the second-order polynomial:

$$y = \alpha_0 + \sum_{i=1}^N \alpha_i x_i + \sum_{i=1}^N \alpha_{ii} x_i^2 + \sum_{i \neq j}^N \alpha_{ij} x_i x_j \quad (5)$$

where  $N$  is the number of design parameters;  $\alpha_0$ ,  $\alpha_i$ ,  $\alpha_{ii}$  and  $\alpha_{ij}$  are the polynomial coefficients and can be determined by the least square method with the help of database sample points which create by DOE.

For DOE, the LHS method was used to construct the database sample points. This method can approximate random sampling from multivariate parameter distribution [25]. First, it divides the sampling unit into different layers according to a certain characteristic or a certain rule, and then draws samples independently and randomly from different layers. Therefore, the structure of the sample is similar to the overall structure, so that a small number of sample points can be used to construct an accurate approximate function between the design parameter and the optimization objective in the entire design space.

NSGA-II [26,27] was used for multi-objective global optimization. Every optimization objective was treated separately in NSGA-II. “Mutation” and “crossover” were used to ensure that the final result is the global optimal solution. “Crowding distance sorting” and “non-dominated sorting” were used to reduce the process complexity and improve the elitism of the strategy.

All the above mentioned softwares are integrated on the Isight 5.8 platform to automatically execute the optimization process. Firstly, select appropriate design parameters and their ranges from



IDM according to the optimization objectives. Secondly, use LHS to construct a proper number of different design parameters combinations in the entire design space as database sample points. Thirdly, use the different design parameter combinations from the second step to generate different impeller through IDM and use ANSYS CFX to calculate the impeller performance. Furthermore, RSM is used to construct the approximate function between the design parameters and optimization objectives. In this step, using ANSYS CFX to calculate impeller performance requires enough time and high computing resources, especially when the database sample point is large. Finally, NSGA-II is used to solve the approximate model to obtain the Pareto optimal solution set.

#### 4. Optimization Settings

##### 4.1. Design Parameters

It can be seen from the introduction of the IDM that the distribution of  $r\overline{V}_\theta$  and stacking conditions are closely related to the blade shape and the pressure distribution. Therefore, the distribution of  $r\overline{V}_\theta$  along spanwise at the impeller exit, the distribution of blade loading along meridional shape at hub and shroud, and stacking were selected to parameterize the impeller, other parameters keep unchanged during the optimization process.

In this study, the second-order parabolic was chosen to describe the SDIEC.

$$r\overline{V}_\theta = a_1 r^2 + b_1 r + c_1 \quad (6)$$

where  $a_1$ ,  $b_1$ , and  $c_1$  are the undetermined coefficients.

To determine the values of  $a_1$ ,  $b_1$ , and  $c_1$ , the value of  $r\overline{V}_\theta$  at three different points in the spanwise of the impeller exit needs to be known. In this study, the value of  $rV_h$  (the value of  $r\overline{V}_\theta$  at hub) and  $rV_s$  (the value of  $r\overline{V}_\theta$  at shroud) are selected as design parameters. The value of  $r\overline{V}_\theta$  at mid-span is automatically determined according to the impeller Euler head. When the values at these three points are determined, the values of  $a_1$ ,  $b_1$ , and  $c_1$  can be calculated. Thus, the unique second-order parabolic equation is established and all the  $r\overline{V}_\theta$  values at other positions of the spanwise can be determined.

Three different  $r\overline{V}_\theta^*$  distribution forms at impeller exit are shown in Figure 6, in this figure,  $r^* = (r - r_{\text{hub}})/(r_{\text{shroud}} - r_{\text{hub}})$  is the normalized spanwise distance at impeller exit and  $r\overline{V}_\theta^* = r\overline{V}_\theta/\omega^2 r_{\text{shroud}}$  is the normalized circulation.

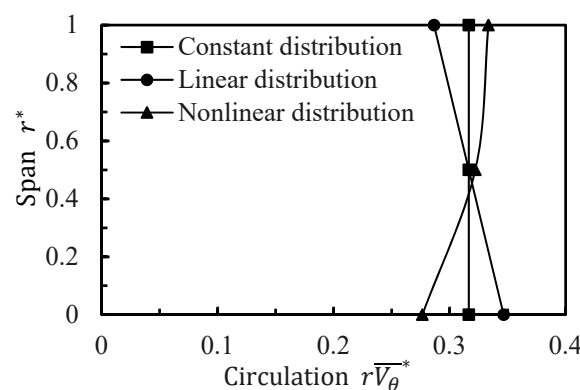


Figure 6. Three different forms of spanwise distribution of impeller exit circulation (SDIEC).

The distribution of blade loading along meridional shape at hub and shroud is a typical “three-segment” distribution as shown in Figure 7, where  $m^* = m/m_{\text{total}}$  is the normalized meridional distance. For each streamline, the distribution of blade loading is determined by the following four parameters,  $DRVT$ ,  $K$ ,  $NC$ , and  $ND$ .  $DRVT$  and  $K$  represent the blade loading at the leading edge and the slope of linear line respectively.  $NC$  and  $ND$  are the locations of the connection points between the

parabolic curve and the straight line. The blade loading at other positions between hub and shroud were determined by linear interpolation.

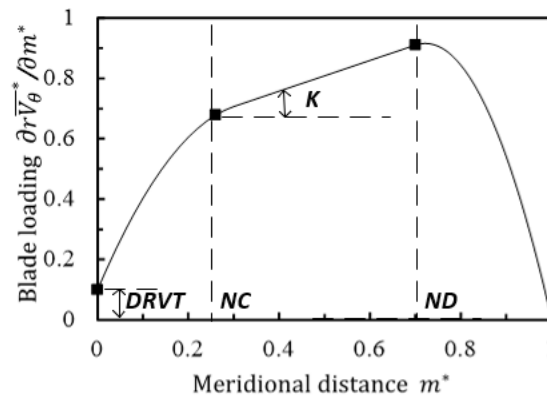


Figure 7. Blade loading distribution.

For mixed-flow pump design, stacking condition is also an important parameter since it can effectively suppress the generation of secondary flow [28,29]. Generally, the stacking  $\beta$  is considered negative if the blade leaned against the rotation direction as shown in Figure 5. With this condition, the pressure at the hub will increase and the pressure at the shroud will decrease.

Therefore, the parameterization of the impeller can be completed by the following eleven parameters:  $rV_h$ ,  $rV_s$ ,  $DRVT_s$ ,  $K_s$ ,  $NC_s$ ,  $ND_s$ ,  $DRVT_h$ ,  $K_h$ ,  $NC_h$ ,  $ND_h$ , and  $\beta$ .

#### 4.2. Optimization Objectives and Constraints

To improve the performance of the mixed-flow pump, the pump efficiency  $\eta$  at  $0.8Q_{des}$  and  $1.2Q_{des}$  were selected as the optimization objectives to enlarge the operating range of the high efficiency area. To make the optimized pump have similar specific speed, higher pump efficiency and better cavitation performance at the design point, the pump head  $H_{1.0}$ , efficiency  $\eta_{1.0}$  and the normalized area of low-pressure area  $A^*$  (the area on the blade surface where pressure is lower than water vaporization pressure 3169 Pa) at  $1.0Q_{des}$  were selected as the constrains. The optimization objective can be calculated by Equation (7), the constrains can be described as Equations (8)–(10):

$$\eta = \frac{(P_{out} - P_{in})Q}{M\omega} \quad (7)$$

$$0.97H_{ori} \leq H_{1.0} = \frac{P_{out} - P_{in}}{\rho g} \leq 1.03H_{ori} \quad (8)$$

$$\eta_{1.0} \geq \eta_{1.0ori} \quad (9)$$

$$A^* = \frac{A_{low}}{A_{ori}} \leq 1 \quad (10)$$

where  $P_{out}$  and  $P_{in}$  are the total pressures at outlet and inlet, respectively;  $M$  is the torque on the impeller;  $\omega$  is the angular velocity of the impeller;  $\rho$  is the density of the fluid;  $g$  is the gravitational acceleration;  $H_{ori}$  is the head of the original model at the design point;  $\eta_{1.0ori}$  is the pump efficiency of the original model at the design point;  $A_{ori}$  is the low-pressure area of the original model at the design point,  $A_{low}$  is the low-pressure area of the optimized model at the design point.

#### 4.3. Algorithm Settings

The number of design parameters  $N$  is one of the important factors that affect the accuracy of the approximated model. Generally, the number of design parameters should be less than ten [30]. After a great number of impeller generation and performance verification, the two parameters  $NC_s$



and  $NC_h$  with the least influence on performance were found and fixed at 0.1 and 0.4 respectively. The remaining nine parameters and ranges are shown in Table 3, and all selected as design parameters.

**Table 3.** Design parameters and ranges.

Variable	$rV_h$	$rV_s$	$DRVT_h$	$DRVT_s$	$K_h$	$K_s$	$ND_h$	$ND_s$	$\beta$
Range	0.3~0.34	0.3~0.34	-0.2~0.2	-0.2~0.2	-1.5~1.5	-1.5~1.5	0.1~0.9	0.4~0.9	-15~15

The other important factor is the number of sampling points. From Equation (5), the least number of sampling points is  $(N + 1) \times (N + 2) / 2$ , however, to make RSM more accurate, the recommended sampling points is twice the number of least sampling points. In this study,  $N$  is 9, hence, 140 sampling points were generated by using LHS. Among those sample points, 110 sampling points were used to construct the approximated model and 30 sampling points were used for error analyses.

The settings of NSGA-II are shown in Table 4. Generally, too small “population size” will lead to difficulty in obtaining the optimal solution, and too large “population size” will result in a slower convergence rate, therefore, the recommended value is between 30 and 160 [31]. The “population size” and “number of generations” are both in the present study are set to 100 with a total of 10,000 different configurations of impellers generated in this step.

**Table 4.** Parameters setting for non-dominated sorting genetic algorithm (NSGA-II).

Setting	Value
Population Size	100
Number of Generations	100
Crossover Probability	0.9
Cross Distribution Index	10
Mutation Distribution Index	20
Initialization Mode	Random

## 5. Results and Discussions

### 5.1. Experimental Validation

The performance estimation of the mixed-flow pump in this optimization process is completed by the CFD calculations. The accuracy of the CFD calculation is crucial to the reliability of the optimization results. In this study, the accuracy of the CFD calculations is proved by comparing the experimental performance and simulation performance of the original model.

The TianJin experiment bench was built to test the pumps used in the South-to-North Water Diversion Project, and it is one of the most accurate experiment benches in China. The overall uncertainty of the experiment bench is less than 0.3%, and the random uncertainty is also less than 0.1%. The experiment performance of the original model was tested by this bench as Figure 8a shows. The performance comparison between the experiment and CFD calculation is shown in Figure 8b. It can be seen that the maximum efficiency deviation does not exceed 2% and the head deviation does not exceed 4%. Therefore, CFD calculation has high accuracy and the optimization result based on CFD calculation is reliable.

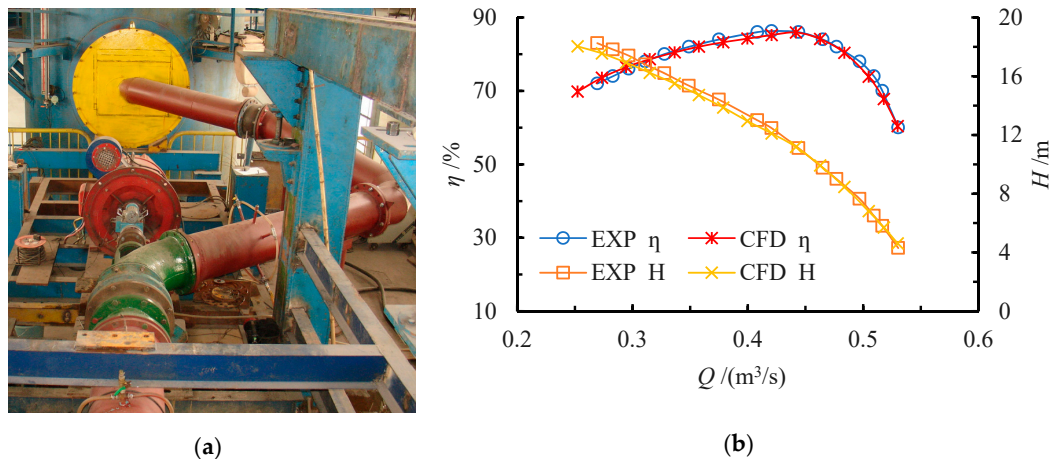


**Figure 8.** Experimental validation (a) Experimental bench and (b) performance comparison between CFD and experimental.

### 5.2. Analysis of the Main Effect

After constructing the approximate model through RSM, the main effect of each parameter on the optimization objective can be analyzed to provide a reference for the selection of parameters and ranges of similar optimization in the future. Figure 9 shows the main effect of the nine design parameters on the two objectives. In this figure, the horizontal axis represents the normalized design parameters range, 0 represents the minimum value of parameters, and 1 represents the maximum value of parameters. Such graphs can be obtained by changing one design parameter, keeping other design parameters unchanged, and plotting the change of optimization objectives with design parameters.

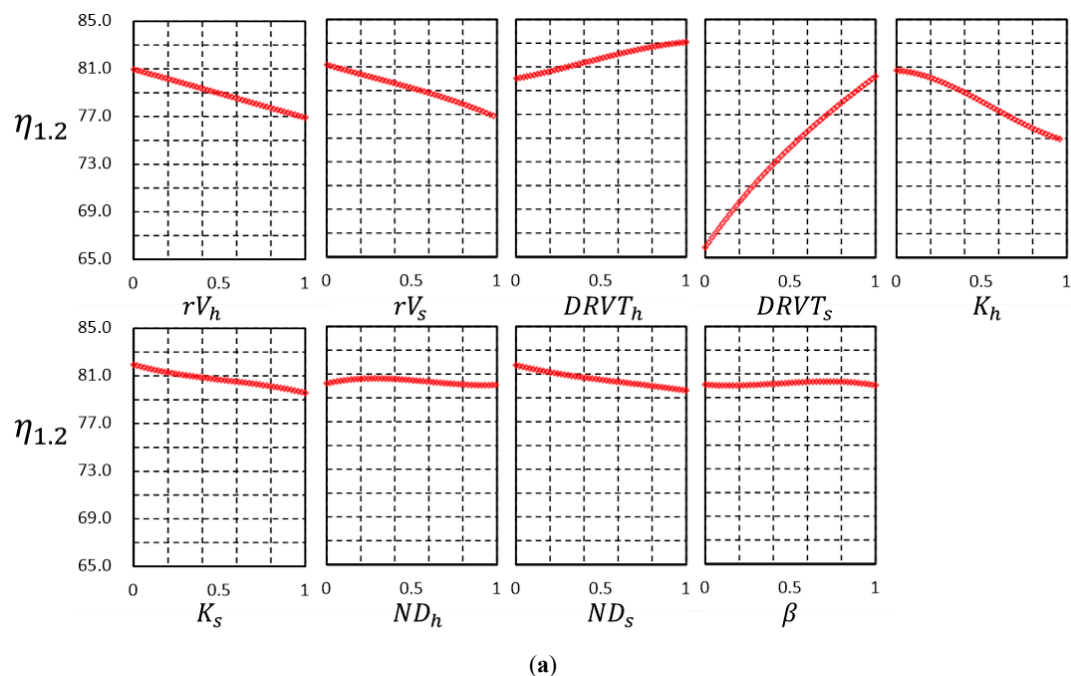


**Figure 9.** Cont.

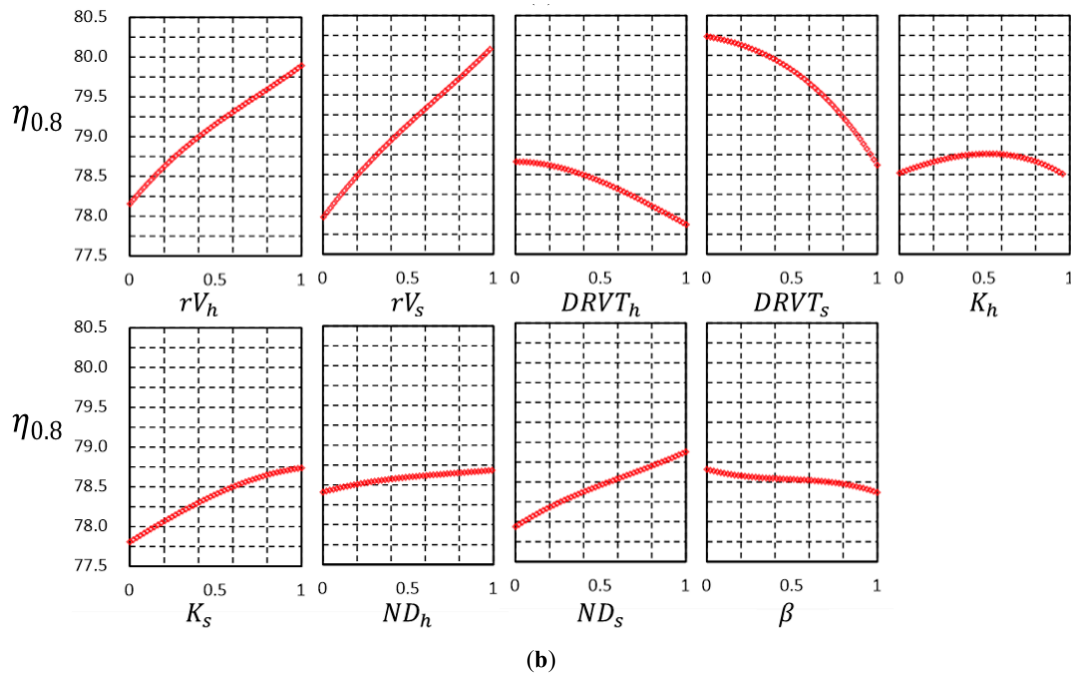


**Figure 9.** Main effect of each design parameter on different optimization objectives (a)  $1.2Q_{des}$  and (b)  $0.8Q_{des}$ .

It can be seen that each parameter has different effects on the two optimization objectives. The contribution of each design parameter to the pump efficiency at  $1.2Q_{des}$  is in the following order:  $DRVTS > K_h > rVs > rVh > DRVTh > K_s > ND_s > ND_h > \beta$ . The contribution of each design parameter to the pump efficiency at  $0.8Q_{des}$  is in the following order:  $rVs > rVh > DRVTS > K_s > ND_s > DRVTh > \beta > ND_h > K_h$ . Therefore, it is necessary to consider  $rVs$  and  $rVh$  in the optimization process after comprehensively considering their effect on the pump performance.

### 5.3. Optimization Results

All the impellers generated by NSGA-II and their corresponding optimization objective values are shown in Figure 10a. In this figure,  $\eta_{0.8}$  and  $\eta_{1.2}$  represent the pump efficiency at  $0.8Q_{des}$  and  $1.2Q_{des}$ , respectively. The red points indicate that the performance of the corresponding mixed-flow pump does not meet the requirement of the constraints. To make the optimization results more intuitive, all the optimal solutions that satisfy the constraints were selected as shown in Figure 10b. It can be seen that the pump efficiency at  $0.8Q_{des}$  and  $1.2Q_{des}$  has a competitive relationship, with the increasing pump efficiency at  $0.8Q_{des}$ , the pump efficiency at  $1.2Q_{des}$  inevitably decreases. According to different selection criteria, three impellers (I1~I3) with different configurations were selected for further study, the selection criteria can be described as Equation (11), where  $\eta_{0.8ori}$  and  $\eta_{1.2ori}$  are the pump efficiency of the original model at  $0.8Q_{des}$  and  $1.2Q_{des}$  respectively.

$$I1 : \begin{cases} \text{Maximum } \eta_{1.2} \\ \eta_{0.8} > \eta_{0.8ori} \end{cases} \quad I2 : (I1 + I3)/2 \quad I3 : \begin{cases} \text{Maximum } \eta_{0.8} \\ \eta_{1.2} > \eta_{1.2ori} \end{cases} \quad (11)$$

The design parameters of impeller I1, I2 and I3 are shown in Table 5, It should be noted that  $rVh$ ,  $rVs$  and  $\beta$  have reached the limits of the given range. Therefore, to further improve the optimization effect, the range of these parameters should be further expanded in the future research.

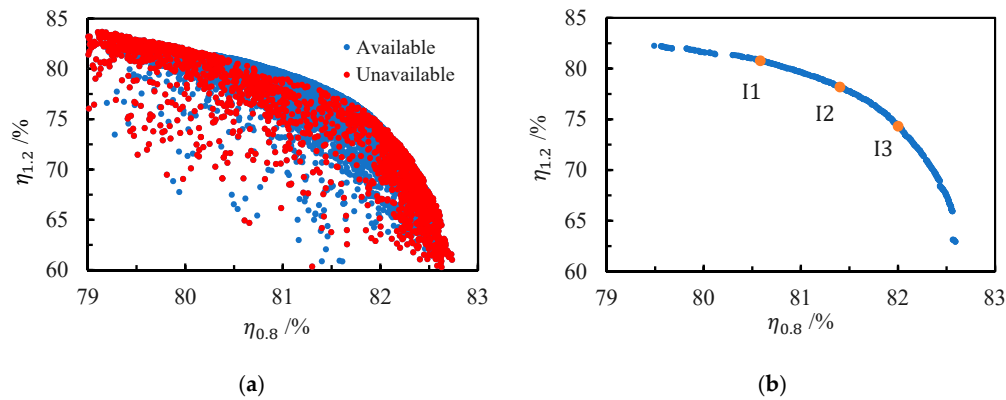


Figure 10. Results of NSGA-II (a) All configurations and (b) Pareto optimal solution.

Table 5. Design parameters of optimization results.

Variable	$rV_h$	$rV_s$	$DRVT_h$	$DRVT_s$	$K_h$	$K_s$	$ND_h$	$ND_s$	$\beta$
I1	0.3363	0.3363	0.1790	0.1925	−0.8935	1.0366	0.2116	0.6057	−14.9394
I2	0.3364	0.3363	0.1956	0.0747	−1.1088	0.6562	0.2601	0.5003	−14.7681
I3	0.3364	0.3365	0.1363	−0.0617	−1.1141	0.3910	0.2937	0.7271	−14.9837

The performance comparison between RSM prediction and CFD calculation for I1, I2, and I3 are shown in Table 6. It can be seen that the performance predicted by RSM agrees well with the CFD calculations. Compared with the original model, the performance of all the selected model has been comprehensively improved and the head change at  $1.0Q_{des}$  was within the acceptable range. Impeller I2 was selected as the preferred impeller when the efficiency, head and cavitation were considered. The SDIEC, and blade loading distribution along meridional shape at hub and shroud of the optimized impeller I2 are shown in Figure 11.

Table 6. Performance comparison.

Impeller \ Performance	RSM		CFD				
	$\eta_{0.8}(\%)$	$\eta_{1.2}(\%)$	$\eta_{0.8}(\%)$	$\eta_{1.2}(\%)$	$H_{1.0}(\text{m})$	$\eta_{1.0}(\%)$	$A^*(\%)$
I1	80.58	80.77	80.40	80.31	11.92	88.72	53.97
I2 (Preferred)	81.40	78.19	81.11	77.62	12.37	88.60	3.08
I3	82.00	74.30	81.31	74.75	12.44	87.68	18.22
Original model			80.48	73.84	12.10	85.21	100

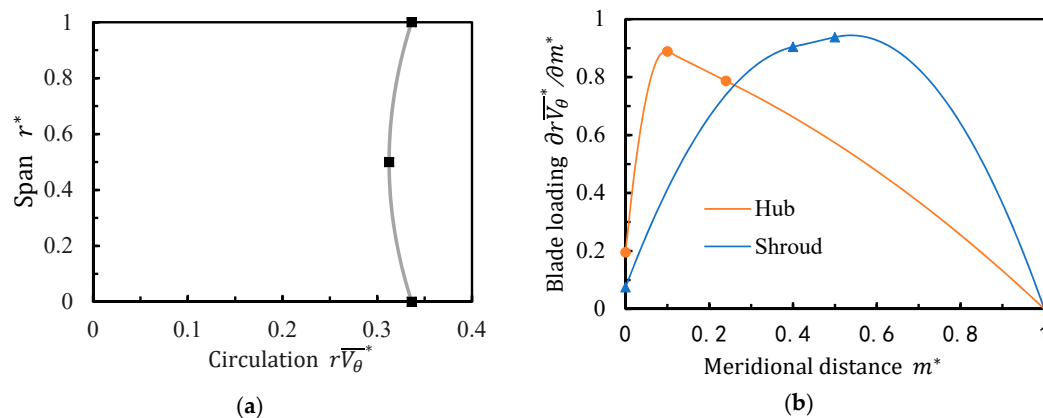


Figure 11. Circulation distribution and blade loading distribution of the optimized impeller I2 (a) spanwise distribution of impeller exit circulation and (b) blade loading distribution along meridional shape at hub and shroud.

#### 5.4. Comparisons between Original and Preferred Impellers

Figure 12 shows the pump efficiency and head comparison between the original and preferred impellers. Compared with the original model, the pump efficiency of preferred impeller has been greatly improved, especially under the large flow condition, and the efficiency at  $0.8Q_{des}$ ,  $1.0Q_{des}$  and  $1.2Q_{des}$  are increased by 0.63%, 3.39%, and 3.77%, respectively. The head deviation at  $1.0Q_{des}$  is less than 1.84%, which meets the design requirements, however, the head at  $0.8Q_{des}$  has decreased by 5.38%.

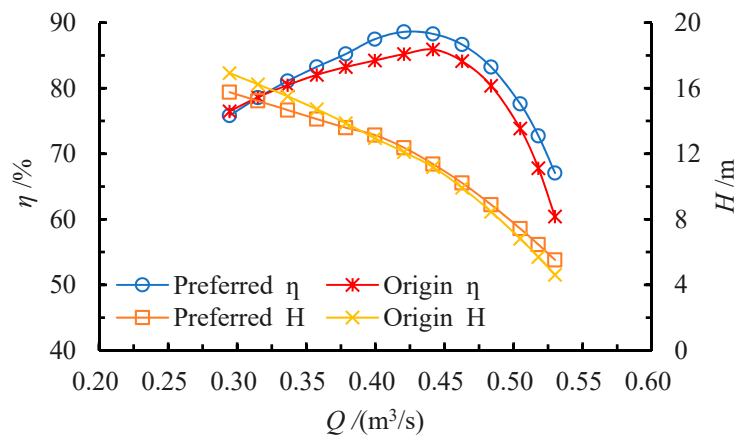


Figure 12. Comparison of performance between the preferred and original model.

Generally, the cavitation on the blade surface is most likely to occur near the shroud, by increasing the pressure at that region, the cavitation can be effectively suppressed. Figure 13 shows the comparison of pressure distribution on the blade working surface and suction surface between the original and preferred impeller at  $1.0Q_{des}$ . Compared with the original model, the low-pressure area of the working surface and suction surface of the preferred impeller blade almost completely disappeared, which means the cavitation performance of the preferred impeller has been improved. In addition, the pressure distribution on the blade surface of the preferred impeller is also more uniform, and the radial adverse pressure gradient is greatly reduced, which helps reduce the radial secondary flow and improve the efficiency of the impeller.

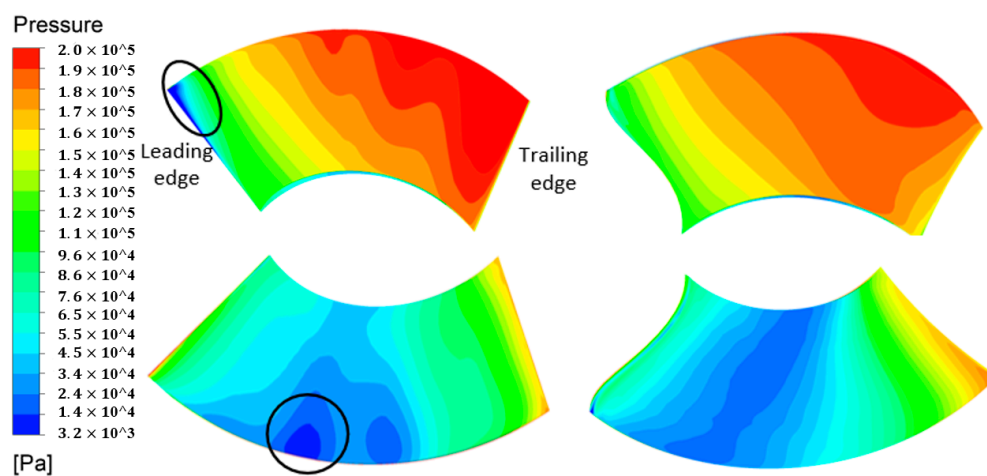
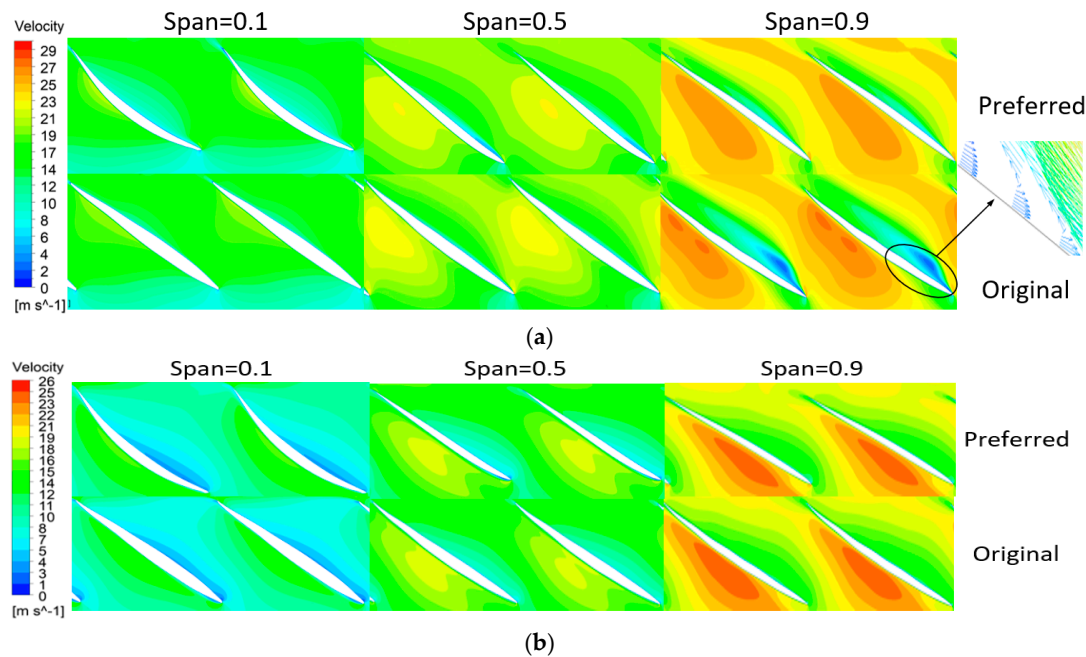


Figure 13. Comparison of pressure distribution on the blade surface (a) original impeller and (b) preferred impeller.

Figure 14 shows the relative velocity distribution in the expansion diagram of turbo surface of the preferred, and original impeller at  $1.2Q_{des}$  and  $0.8Q_{des}$ , these data are extracted at the  $r^* = 0.1$ ,

0.5 and 0.9 after considering the viscous effect caused by the friction between the fluid and the wall. It can be seen from Figure 14a that at  $1.2Q_{des}$  of the original impeller, the relative velocity distribution at the blade-to-blade channel is not uniform, especially at the leading edge of the blade where is close to the shroud. There is an obvious low-speed area accompanied by backflow phenomenon. After optimization, the non-uniformity of the relative velocity distribution among the blade-to-blade channel is reduced and the low-speed area is completely suppressed. The same phenomenon was observed in Figure 14b, the difference is that the low-speed area has changed from the shroud to the hub, and there is no backflow in the low-speed area.



**Figure 14.** Comparison of relative velocity distribution at different span (a)  $1.2Q_{des}$  and (b)  $0.8Q_{des}$ .

Considering the impact of the downstream components of the impeller on the pump efficiency, the uniformity of the velocity distribution of the impeller outlet possibly is another factor that has a greater influence on the pump efficiency. Figure 15 shows the velocity distribution at the outlet of the original and preferred impeller at  $0.8Q_{des}$  and  $1.2Q_{des}$ . It can be seen that at  $1.2Q_{des}$ , the velocity distribution at the outlet of the preferred impeller becomes more uniform, especially the high-velocity area near the shroud side is eliminated. The same phenomenon was observed at  $0.8Q_{des}$ , the difference is that the high-velocity area is weakened at both the hub and shroud.

To some extent, the spanwise distribution of impeller exit total pressure represents the working ability of the blade at different blade heights. Figure 16 shows the spanwise distribution of impeller exit total pressure of the original and preferred impeller at  $0.8Q_{des}$  and  $1.2Q_{des}$ . It can be seen that compared with the original impeller, the total pressure on the hub side of the preferred impeller is increased, the total pressure at the shroud side is reduced, and the spanwise distribution of impeller exit total pressure becomes more uniform. This means that the mixing loss due to uneven total pressure distribution in the impeller will be reduced, and the possibility of cavitation at shroud is also reduced since the total pressure at the shroud is reduced.



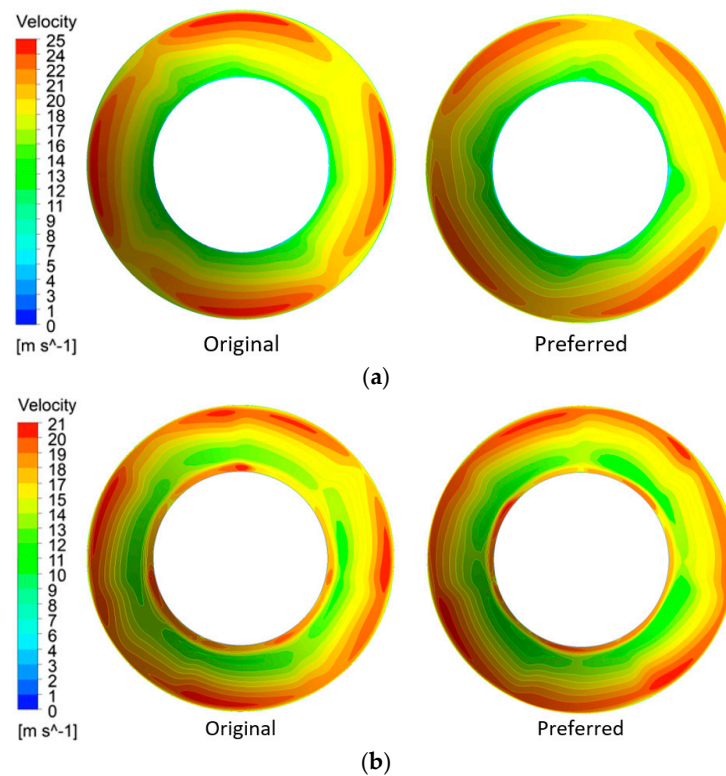


Figure 15. Comparison of velocity distribution at impeller exit (a)  $1.2Q_{des}$  and (b)  $0.8Q_{des}$ .

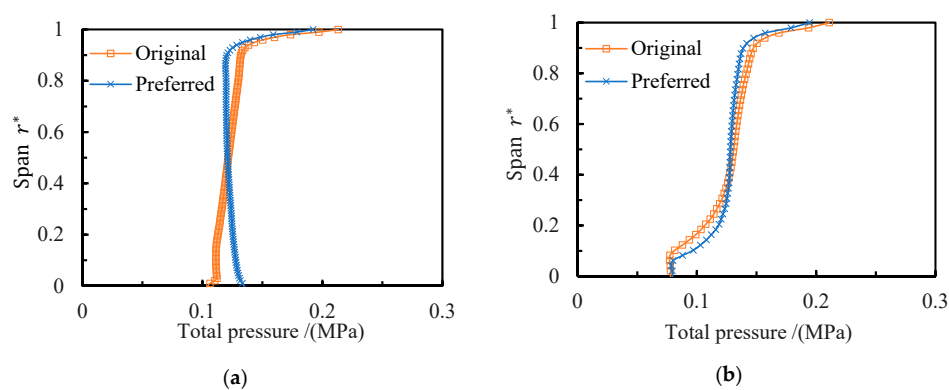


Figure 16. Comparison of total pressure distribution at impeller exit (a)  $1.2Q_{des}$  and (b)  $0.8Q_{des}$ .

## 6. Conclusions

In this study, a mixed-flow pump which is presently used in the South-to-North Water Diversion Project is optimized using a combined optimization system. The impeller was parameterized by IDM, and the circulation, blade loading, and stacking were selected as the design parameters. The pump efficiency at  $0.8Q_{des}$  and  $1.2Q_{des}$  were selected as the optimization objectives while the head, efficiency and area of low-pressure area at  $1.0Q_{des}$  were selected as constraints. The results of this study can be summarized as follows:

- (1) The CFD calculations accurately simulated the flow in the pump, and the performance curves agreed well with the experimental curves. The maximum efficiency and head deviations did not exceed 2% and 4% respectively.
- (2) The optimization results show that the non-linear SDIEC is better than the constant and linear distributions. The analysis of the main effect also shows that  $rV_s$  and  $rV_h$  have a greater impact on the performance of the mixed-flow pump impeller than other design parameters. Therefore,

it is necessary to take  $rV_s$  and  $rV_h$  as design parameters in the optimization process to further improve the performance of the mixed-flow pump impeller.

- (3) The pump efficiency with preferred impeller at  $0.8Q_{des}$ ,  $1.0Q_{des}$ , and  $1.2Q_{des}$  are 81.11%, 88.60%, and 77.62%, respectively. Compared with the original model, these efficiencies increased by 0.63%, 3.39%, and 3.77%, respectively. At the same time, the cavitation performance of preferred impeller has been significantly improved. The area of low-pressure region further reduced by 96.92% and the pump head deviation at  $1.0Q_{des}$  is less than 1.84%, which is within an acceptable range.

Therefore, the design method proposed in this paper can reliably and effectively improve the comprehensive performance of the mixed-flow pump under the premise of small head changes.

**Author Contributions:** Conceptualization, M.W.; methodology, M.W. and F.M.; validation, M.W. and Y.L.; data curation, M.W. and Y.L.; writing—original draft preparation, M.W.; writing—review and editing, J.C., D.A., and J.Y.; supervision, Y.L. and J.Y.; project administration, Y.L. and J.Y.; All authors have read and agreed to the published version of the manuscript.

**Funding:** This research was funded by National Key Research and Development Plan (Grant No. 2018YFB0606103), Science and Technology Plan of Wuhan (Grant No.2018060403011350).

**Acknowledgments:** The author sincerely thanks the support of the research center of fluid mechanical engineering technology of Jiangsu University.

**Conflicts of Interest:** The authors declare no conflict of interest.

## Nomenclature

$n_s$	specific speed
$H$	head
$N$	rotational speed
$Q$	volume flow rate
$\overline{V}_\theta$	tangentially velocity
$r$	radius or radial direction
$B$	blade numbers
$p^+$	static pressure at blade work surface
$p^-$	static pressure at blade suction surface
$W_m$	relative velocity on the blade surface
$m$	streamline in the meridional shape or meridional distance
$\overline{V}_z$	axial components of the circumferential average absolute velocity
$\overline{V}_r$	radial components of the circumferential average absolute velocity
$v_{zbl}$	axial component of periodic velocity
$v_{rbl}$	radial component of periodic velocity
$v_{\theta bl}$	circumferential component of periodic velocity
$f$	wrap angle
$V_h$	tangentially velocity at hub
$V_s$	tangentially velocity at shroud
$r^*$	normalized spanwise distance
$\overline{V}_\theta^*$	normalized tangentially velocity
$m^*$	normalized meridional distance
DRVT	blade loading at leading edge
NC	fore connection points
ND	aft fore connection points
$K$	slope of linear line
$\beta$	stacking condition
$\eta$	pump efficiency
$A^*$	normalized area of low-pressure area
$P$	pressure at inlet or outlet
$M$	torque on the impeller
$\omega$	angular velocity of the impeller
$\rho$	density of the fluid
$g$	gravitational acceleration

## Abbreviations

SDIEC	spanwise distribution of impeller exit circulation
CFD	computational fluid dynamics
LHS	Latin hypercube sampling
RSM	response surface model
NSGA-II	non-dominated sorting genetic algorithm
DOE	design of experiment
CCD	central composite design
RANS	Reynolds average Navier–Stokes

## References

1. Suh, J.-W.; Yang, H.-M.; Kim, Y.-I.; Lee, K.-Y.; Kim, J.-H.; Joo, W.-G.; Choi, Y.-S. Multi-objective optimization of a high efficiency and suction performance for mixed-flow pump impeller. *Eng. Appl. Comput. Fluid Mech.* **2019**, *13*, 744–762. [\[CrossRef\]](#)
2. Kim, S.; Jeong, U.-B.; Lee, K.-Y.; Kim, J.-H.; Yoon, J.-Y.; Choi, Y.-S. Multi-objective optimization for mixed-flow pump with blade angle of impeller exit and diffuser inlet. *J. Mech. Sci. Technol.* **2017**, *31*, 5099–5106. [\[CrossRef\]](#)
3. Pei, J.; Wang, W.; Yuan, S. Multi-point optimization on meridional shape of a centrifugal pump impeller for performance improvement. *J. Mech. Sci. Technol.* **2016**, *30*, 4949–4960. [\[CrossRef\]](#)
4. Shim, H.-S.; Kim, K.-Y.; Choi, Y.-S. Three-objective optimization of a centrifugal pump to reduce flow recirculation and cavitation. *J. Fluids Eng.* **2018**, *140*, 091202. [\[CrossRef\]](#)
5. Shim, H.-S.; Afzal, A.; Kim, K.-Y.; Jeong, H.-S. Three-objective optimization of a centrifugal pump with double volute to minimize radial thrust at off-design conditions. *Proc. Inst. Mech. Eng. Part A J. Power Energy.* **2016**, *230*, 598–615. [\[CrossRef\]](#)
6. Miao, F.; Park, H.-S.; Kim, C.; Ahn, S. Swarm intelligence based on modified PSO algorithm for the optimization of axial-flow pump impeller. *J. Mech. Sci. Technol.* **2015**, *29*, 4867–4876. [\[CrossRef\]](#)
7. Meng, F.; Li, Y.; Yuan, S.; Wang, W.; Zheng, Y.; Osman, M.K. Multiobjective Combination Optimization of an Impeller and Diffuser in a Reversible Axial-Flow Pump Based on a Two-Layer Artificial Neural Network. *Processes* **2020**, *8*, 309. [\[CrossRef\]](#)
8. Yang, W.; Xiao, R. Multiobjective optimization design of a pump–turbine impeller based on an inverse design using a combination optimization strategy. *J. Fluids Eng.* **2014**, *136*, 249–256. [\[CrossRef\]](#)
9. Zangeneh, M. A compressible 3D design method for radial and mixed flow turbomachinery blades. *Int. J. Numer. Methods Fluids* **1991**, *13*, 599–624. [\[CrossRef\]](#)
10. Daneshkhah, K.; Zangeneh, M. Parametric design of a Francis turbine runner by means of a three-dimensional inverse design method. *IOP Conf. Ser. Earth Environ. Sci.* **2010**, *12*, 012058. [\[CrossRef\]](#)
11. Peng, G. A practical combined computation method of mean through-flow for 3d inverse design of hydraulic turbomachinery blades. *J. Fluids Eng.* **2005**, *127*, 1183–1190. [\[CrossRef\]](#)
12. Zangeneh, M.; Goto, A.; Harada, H. On the Design Criteria for Suppression of Secondary Flows in Centrifugal and Mixed Flow Impellers. *J. Turbomach.* **1998**, *120*, 723. [\[CrossRef\]](#)
13. Zhu, B.; Tan, L.; Wang, X.; Ma, Z. Investigation on flow characteristics of pump-turbine runners with large blade lean. *J. Fluids Eng.* **2017**, *140*, 031101. [\[CrossRef\]](#)
14. Yin, J.; Wang, D. Review on applications of 3D inverse design method for pump. *Chin. J. Mech. Eng.* **2014**, *27*, 520–527. [\[CrossRef\]](#)
15. Zhu, B.; Wang, X.; Tan, L.; Zhou, D.; Zhao, Y.; Cao, S. Optimization design of a reversible pump-turbine runner with high efficiency and stability. *Renew. Energy* **2015**, *81*, 366–376. [\[CrossRef\]](#)
16. Liu, L.; Zhu, B.; Bai, L.; Liu, X.; Zhao, Y. Parametric design of an ultrahigh-head pump-turbine runner based on multiobjective optimization. *Energies* **2017**, *10*, 1169. [\[CrossRef\]](#)
17. Ma, Z.; Zhu, B.; Rao, C.; Shangguan, Y. Comprehensive hydraulic improvement and parametric analysis of a francis turbine runner. *Energies* **2019**, *12*, 307. [\[CrossRef\]](#)
18. Bonaiuti, D.; Zangeneh, M. On the coupling of inverse design and optimization techniques for the multiobjective, multipoint design of turbomachinery blades. *J. Turbomach.* **2009**, *131*, 134–149. [\[CrossRef\]](#)

19. Lee, K.-Y.; Choi, Y.-S.; Kim, Y.-L.; Yun, J.-H. Design of axial fan using inverse design method. *J. Mech. Sci. Technol.* **2008**, *22*, 1883–1888. [[CrossRef](#)]
20. Lang, J. Preliminary study of the optimal distribution law of axial-flow pump impeller axial speed and circulation. *Fluid Mach.* **1990**, *31*. (In Chinese)
21. Chen, L. The Optimal Design Method of Axial Flow Pump Outlet Circumference Variation Law and Geometric Parameter Integration. *Hydraulic Vane Pump.* **1993**, *1*, 27. (In Chinese)
22. Zhang, D.; Li, T.; Shi, W.; Zhang, H.; Zhang, G. Experimental investigation of meridional velocity and circulation in axial-flow impeller outlet. *Trans. Chin. Soc. Agric. Eng.* **2012**, *28*, 73–77. (In Chinese)
23. Zhang, D.; Shi, W.; Li, T.; Gao, X.; Guan, X. Establishment and Experiment on Nonlinear Circulation Mathematical Model of Axial Flow Pump Impeller. *Trans. Chin. Soc. Agric. Mach.* **2013**, *44*, 58–61. (In Chinese)
24. Menter, F.R. Two-equation eddy-viscosity turbulence models for engineering applications. *AIAA J.* **1994**, *32*, 1598. [[CrossRef](#)]
25. Kim, J.-H.; Kim, K.-Y. Analysis and optimization of a vaned diffuser in a mixed flow pump to improve hydrodynamic performance. *J. Fluids Eng.* **2012**, *134*, 071104. [[CrossRef](#)]
26. Gen, M.; Cheng, R. *Genetic Algorithms & Engineering Optimization*; John Wiley & Sons Ltd.: New York, NY, USA, 1999.
27. Lee, D.S.; Gonzalez, L.F.; Periaux, J.; Srinivas, K. Robust design optimization using multi-objective evolutionary algorithms. *Comput Fluids.* **2008**, *37*, 565–583. [[CrossRef](#)]
28. Zangeneh, M.; Goto, A.; Takemura, T. Suppression of Secondary Flows in a Mixed-Flow Pump Impeller by Application of Three-Dimensional Inverse Design Method: Part 1—Design and Numerical Validation. *J. Turbomach.* **1996**, *118*, 536–543. [[CrossRef](#)]
29. Goto, A.; Takemura, T.; Zangeneh, M. Suppression of Secondary Flows in a Mixed-Flow Pump Impeller by Application of Three-Dimensional Inverse Design Method: Part 2—Experimental Validation. *J. Turbomach.* **1996**, *118*, 544–551. [[CrossRef](#)]
30. Miyauchi, S.; Zhu, B.; Luo, X.; Piao, B.; Matsumoto, H.; Sano, M.; Kassai, N. Optimization and Inverse Design of Pump Impeller. *IOP Conf. Ser. Earth Environ. Sci.* **2012**, *15*, 032032. [[CrossRef](#)]
31. Deb, K.; Pratap, A.; Agarwal, S.; Meyarivan, T. A fast and elitist multiobjective genetic algorithm: NSGA-II. *IEEE Trans. Evol. Comput.* **2002**, *6*, 182–197. [[CrossRef](#)]



© 2020 by the authors. Licensee MDPI, Basel, Switzerland. This article is an open access article distributed under the terms and conditions of the Creative Commons Attribution (CC BY) license (<http://creativecommons.org/licenses/by/4.0/>).